

Efficient numerical approach to high-fidelity phase-modulated gates in long chains of trapped ions

Sheng-Chen Liu ¹, Lin Cheng ^{1,4}, Gui-Zhong Yao ^{1,4}, Ying-Xiang Wang ¹, and Liang-You Peng ^{1,2,3,4,*}

¹*State Key Laboratory for Mesoscopic Physics and Frontiers Science Center for Nano-optoelectronics, School of Physics, Peking University, 100871 Beijing, China*

²*Collaborative Innovation Center of Quantum Matter, Beijing 100871, China*

³*Collaborative Innovation Center of Extreme Optics, Shanxi University, 030006 Taiyuan, China*

⁴*Beijing Academy of Quantum Information Sciences, Beijing 100193, China*



(Received 11 January 2023; accepted 2 March 2023; published 22 March 2023)

Almost every quantum circuit is built with two-qubit gates in the current stage, which are crucial to the quantum computing in any platform. The entangling gates based on Mølmer-Sørensen schemes are widely exploited in the trapped-ion system, with the utilization of the collective motional modes of ions and two laser-controlled internal states, which are served as qubits. The key to realize high-fidelity and robust gates is the minimization of the entanglement between the qubits and the motional modes under various sources of errors after the gate operation. In this work, we propose an efficient numerical method to search high-quality solutions for phase-modulated pulses. Instead of directly optimizing a cost function, which contains the fidelity and the robustness of the gates, we convert the problem to the combination of linear algebra and the solution to quadratic equations. Once a solution with the gate fidelity of 1 is found, the laser power can be further reduced while searching on the manifold where the fidelity remains 1. Our method largely overcomes the problem of the convergence and is shown to be effective up to 60 ions, which suffices the need of the gate design in current trapped-ion experiments.

DOI: [10.1103/PhysRevE.107.035304](https://doi.org/10.1103/PhysRevE.107.035304)

I. INTRODUCTION

Among the platforms promising to achieve a universal quantum computation, the trapped-ion system has some specific advantages. The coherence time comes first. In current experiments, the coherence time of a single qubit has exceeded 1 hour [1], which is at least seven orders of magnitude longer than the operation time of quantum gates. The full connectivity is another outstanding character, which has been recently realized in the experiment for 11 ions [2]. This property can improve the implementation efficiency of many quantum algorithms, such as the quantum Fourier transform [3], in which much more quantum gates would have to be used without the full connectivity. Meanwhile, the fidelities of the quantum operations are quite competitive, which have reached 99.99% and 99.9% for single-qubit gates and two-qubit gates, respectively [4,5].

Nowadays, scientists are focusing on the scalability of the trapped-ion system to more and more qubits which can be coherently operated. The linear chain is the most popular configuration and the entanglement was established among more than 20 ions in a chain [6]. The two-qubit gates are also frequently demonstrated on ion chains [7,8]. In the future, there are several technical routes to the goal of scalability. Two-dimensional or three-dimensional arrays of ions are explored to accommodate more qubits, but they will also suffer

from more serious micromotion, which is a big challenge for high-fidelity gates [9–11]. The ion shuttling can be used to separate and operate several targeted ions each time and other qubits are stored in other regions, which means that the number of the total qubits can be improved, while the electronic control is supposed to be very complicated [12,13]. Another technique along with a large-scale quantum computation is the realization of global and parallel entangling gates [8,14]. These efficient gates can significantly cut down the amount of the gates used in some algorithms. However, ion chains and two-qubit gates still have huge potentials to be explored. More than 100 ions have been trapped in a chain, but the number of ions that can be coherently operated is yet to be increased [15]. As for two-qubit gates, they play an important role in many algorithms, even with the participation of the global and parallel gates. Therefore, the careful design of two-qubit gates, which are robust to all kinds of experimental error sources in long chains, is the critical issue in the scalable quantum computation with the trapped-ion system.

To realize this goal, many schemes based on Mølmer-Sørensen (MS) gates [16,17] and different pulse designs were proposed in which two qubits were entangled through the amplitude [7,18,19], the phase [14,20,21], or the frequency [22,23] modulated pulses with many time segments or continuously modulated pulses [24,25]. Some of the gates were robust to the experimental errors, such as the drifts of the mode frequencies [23,25].

In this work, we focus on the phase-modulated pulses, which can be experimentally controlled with a high precision

*liangyou.peng@pku.edu.cn

[14]. Although the analytic scheme [20] and the numerical optimization [21,26] are both available, they face the challenging problem of scalability. To be specific, the analytic scheme leads to an exponential increase of pulse segments and the numerical optimization is a highly nonlinear optimization problem, which is difficult to obtain the targeted solutions for long chains. Here, we propose an efficient numerical framework, which is capable of searching the optimal solutions of high-fidelity two-qubit gates for long chains of ions. Our method is based on converting the optimization to the combination of linear algebra and the solution to quadratic equations, which is shown to largely improve the convergence of the optimization. We find that the good performance of the gates, such as the robustness and the low laser power can be nicely kept when the number of ions increases. Moreover, the fidelity and the scalability are greatly improved when the laser power and the gate time of our scheme are similar to the previous ones.

The rest of the paper is organized as follows. In Sec. II, the theory of MS gates is briefly reviewed and our numerical framework of the phase-modulated scheme is introduced. Then, in Sec. III, some examples of the gates and their performances are presented. In particular, the scalability of our scheme is also discussed in detail. Finally, in Sec. IV, we draw a short conclusion and discuss the possible improvement with the consideration of more realistic experimental conditions.

II. THEORETICAL AND NUMERICAL METHODS

In this section, we will first present the theoretical framework of the basic Mølmer-Sørensen scheme. Then, for the realization of the phased-modulated MS gates, we will show how we can convert the optimization problem into the combination of linear algebra and the solution to quadratic equations. Finally, we will formulate the additional power optimization scheme.

A. Basic Mølmer-Sørensen scheme

We begin with a brief review of MS gates, which are widely used to entangle two qubits for trapped ions. In MS gates, the phase-insensitive configuration is usually used, where the driving fields on each ion are composed of three laser beams and two of them have overlapping wave vectors [14,19,27]. Furthermore, one of the lasers is global and the other two lasers are split to address the two target ions, in which case we can ensure the fields felt by the two ions are kept proportional at any time. Hence, we can use only one equivalent Rabi frequency in the MS model.

Considering the motion of the chain with N ions aligned along the z axis, we know that there are N axial modes in the z axis and $2N$ radial modes in the xy plane. In current experiments, radial modes are preferred due to their insensitivity to the ion heating [7,28]. Thus, in the present work, we only discuss radial modes, which means that the wave vector \mathbf{k} of the laser beam is in the xy plane. As it is known, the symmetry of the trap in the xy plane leads to the mode degeneracy in the x and the y directions. On the contrary, if the trap is asymmetric and thus \mathbf{k} does not lie in the principle axes, modes in the x and y direction with different frequen-

cies can be simultaneously stimulated. In this work, we will consider two cases: for the symmetric case, the laser beams propagate along the $\pm x$ direction and N modes are considered; for the asymmetric case, the laser beams propagate along the diagonal line of the x axis and the y axis and $2N$ modes are considered.

In the interaction picture, the qubit-motion Hamiltonian can be expressed as [19]

$$\hat{H}(t) = \hbar\Omega(t) \sin[\mu t + \phi(t)] \sum_{j=j_1, j_2} \sum_k \eta_k b_k^j (\hat{a}_k e^{-i\omega_k t} + \hat{a}_k^\dagger e^{i\omega_k t}) \hat{\sigma}_x^j, \quad (1)$$

where $\Omega(t)$ and $\phi(t)$ are, respectively, the Rabi frequency and the phase of the driving field on the two ions (j_1, j_2), and μ is the detuning from the frequency corresponding to the two internal energy levels of the ions. In Eq. (1), \hat{a}_k and \hat{a}_k^\dagger are annihilation and creation operators for the k th motional mode with the frequency ω_k and the normalized mode vector b_k^j , where k runs over the N or $2N$ modes as concerned. In our calculations, the Lamb-Dicke parameter $\eta_k = \Delta k_\nu \sqrt{\frac{\hbar}{2M_{\text{ion}}\omega_k}} \ll 1$, where M_{ion} is the mass of a single ion and Δk_ν is the ν -axis component of the difference of two wave vectors with ν being the direction related to the k th mode. In addition, the ions are in the quadratic pseudopotential and ω_k and b_k^j can be conveniently obtained by solving an eigenvalue problem [29].

Under the Hamiltonian of Eq. (1), the time evolution at the gate operation time τ is given by

$$\hat{U}(\tau) = \exp \left\{ i \sum_{j=j_1, j_2} \sum_k [\alpha_k^j(\tau) \hat{a}_k^\dagger - \alpha_k^{j*}(\tau) \hat{a}_k] \hat{\sigma}_x^j - i\Theta(\tau) \hat{\sigma}_x^{j_1} \hat{\sigma}_x^{j_2} \right\}, \quad (2)$$

where

$$\alpha_k^j(\tau) = -\eta_k b_k^j \int_0^\tau \Omega(t_\alpha) \sin[\mu t_\alpha + \phi(t_\alpha)] e^{i\omega_k t_\alpha} dt_\alpha, \quad (3)$$

describes the residual entanglement between the ion j and the mode k after the gate and

$$\Theta(\tau) = 2 \sum_k \eta_k^2 b_k^{j_1} b_k^{j_2} \int_0^\tau dt_\alpha \int_0^{t_\alpha} dt_\beta \Omega(t_\alpha) \Omega(t_\beta) \times \sin[\omega_k(t_\alpha - t_\beta)] \sin[\mu t_\alpha + \phi(t_\alpha)] \times \sin[\mu t_\beta + \phi(t_\beta)], \quad (4)$$

is the coupling strength between the ions j_1 and j_2 . The essential requirement for an ideal gate is to decouple the qubits and the motional modes, which means that $\alpha_k^j(\tau) = 0$ and $\Theta(\tau) = \pm\pi/4$. When it comes to the robustness of the gate against errors of motional-mode frequencies (e.g., caused by the stray field [30]), which is a main cause of the infidelity, we can add additional derivative conditions for $\alpha_k^j(\tau)$ [25]:

$$\begin{aligned} \frac{\partial^p \alpha_k^j(\tau)}{\partial \omega_k^p} &= -i^p \eta_k b_k^j \int_0^\tau \Omega(t_\alpha) t_\alpha^p \sin[\mu t_\alpha + \phi(t_\alpha)] e^{i\omega_k t_\alpha} dt_\alpha \\ &= 0, \quad p = 0, 1, \dots, P, \end{aligned} \quad (5)$$

where P is the largest order of robustness.

The fluctuations of motional-mode frequencies are usually quasistatic and hence the deviation of Θ from $\pm\pi/4$ can usually be compensated for by scaling the Rabi frequency $\Omega(t)$ in the experiment [21]. Therefore, in this work, we only focus on α_k^j . If α_k^j at time τ deviates from 0, the fidelity of the MS gate will be lower than 1 and the infidelity can be evaluated by the following equation [19]:

$$1 - F \approx \frac{4}{5} \sum_k (|\alpha_k^{j_1}|^2 + |\alpha_k^{j_2}|^2)(2\bar{n}_k + 1), \quad (6)$$

where \bar{n}_k is the averaged phonon number of the k th mode.

B. Phase-modulated solutions

In the realization of phase-modulated MS gates, the whole $[0, \tau]$ pulse is equally divided into S segments. The Rabi frequency Ω is kept the same during the gate operation, while we can vary the laser phase ϕ_s in each segment $t \in [t_s, t_{s+1})$ where $t_s = s\tau/S$. As discussed in the last subsection, the phases $(\phi_1, \phi_2, \dots, \phi_S)$ should satisfy the disentanglement and the robustness conditions up to the P th order. In this case, Eqs. (3) and (5) can be reduced to

$$\sum_{s=0}^{S-1} \int_{t_s}^{t_{s+1}} t^p \sin(\mu t_\alpha + \phi_s) e^{i\omega_k t_\alpha} dt_\alpha = 0, \quad (7)$$

where $p = 0, 1, \dots, P$ and $k = 1, 2, \dots, N_\omega$ with N_ω being the number of modes equal to N or $2N$ depending on the symmetry of the trap. As can be seen, we now have $2(P+1)N_\omega$ real constraints given by Eq. (7).

Furthermore, some symmetry conditions for the laser pulse can cut down half of the constraint equations (see Appendix A for details). Here, we assume the pulse to be odd [$\phi(t) = -\phi(\tau - t)$] and the number of segments to be even ($S = 2M$ where M is an integer). In addition, we also need μ to satisfy

$$\mu = \frac{(2N_\mu + 1)\pi}{\tau}, \quad N_\mu \in \mathbb{N}. \quad (8)$$

In this case, Eq. (7) can be further simplified to

$$\begin{aligned} \sum_{s=0}^{M-1} \int_{t_s}^{t_{s+1}} t^p \cos(\mu t - \phi_{M-s}) \cos(\omega_k t) dt &= 0, \\ p = 2N_p \leq P, \quad N_p \in \mathbb{N}, \quad k = 1, 2, \dots, N_\omega; \\ \sum_{s=0}^{M-1} \int_{t_s}^{t_{s+1}} t^p \cos(\mu t - \phi_{M-s}) \sin(\omega_k t) dt &= 0, \\ p = 2N_p + 1 \leq P, \quad N_p \in \mathbb{N}, \quad k = 1, 2, \dots, N_\omega, \end{aligned} \quad (9)$$

where the number of real constraints has been cut down to $(P+1)N_\omega$.

The variables ϕ_s seem troublesome in Eq. (9) because the equations nonlinearly depend on ϕ_s . If we put $\cos \phi_s$ and $\sin \phi_s$ into column vectors \mathbf{X}, \mathbf{Y} [31] and combine them to a vector Φ :

$$\mathbf{X} = \begin{pmatrix} \cos \phi_1 \\ \cos \phi_2 \\ \dots \\ \cos \phi_M \end{pmatrix}, \quad \mathbf{Y} = \begin{pmatrix} \sin \phi_1 \\ \sin \phi_2 \\ \dots \\ \sin \phi_M \end{pmatrix}, \quad \Phi = \begin{pmatrix} \mathbf{X} \\ \mathbf{Y} \end{pmatrix}, \quad (10)$$

then Eq. (9) can be written into a matrix form

$$\begin{pmatrix} \mathbf{M}_X^0 & \mathbf{M}_Y^0 \\ \mathbf{M}_X^1 & \mathbf{M}_Y^1 \\ \vdots & \vdots \\ \mathbf{M}_X^P & \mathbf{M}_Y^P \end{pmatrix} \begin{pmatrix} \mathbf{X} \\ \mathbf{Y} \end{pmatrix} = \mathbf{0}, \quad (11)$$

where \mathbf{M}_X^p is the block related to $\cos \phi_s$ in the p th-order robustness conditions and \mathbf{M}_Y^p is similar (see Appendix B for the explicit expressions for matrix elements). The entire coefficient matrix can be denoted as \mathbf{M} .

The phase optimization for the MS gates is reduced to the efficient solution to Eq. (11). The key points of our numerical method are as follows. In the first step, \mathbf{X} and \mathbf{Y} are regarded as independent variables. We find the null space W of \mathbf{M} in which Φ take their values. Next, the constraints of the phase-modulation scheme for each segment are considered, i.e.,

$$\cos^2 \phi_s + \sin^2 \phi_s = 1, \quad s = 1, 2, \dots, M. \quad (12)$$

We note that, once the basis of W is chosen, Φ can be linearly represented with a set of coefficients. Thus, Eq. (12) leads to M quadratic equations of the coefficients, which can be effectively solved by the Newton method. We emphasize that this approach can avoid some convergence problems in the conventional optimization method [21,26] where the cost function depending on variables ϕ_m may have lots of pits which impede the search for the minimum. Moreover, Eq. (12) can be exactly satisfied and thus the resulting fidelity can be kept as 1 without any loss due to numerical errors in the calculations.

More details of the method are necessary to be explained. One important issue is the degree of freedom. We have $2M$ variables and $(P+1)N_\omega$ constraints in Eq. (11), so the dimension of W is $D_1 = 2M - (P+1)N_\omega$. Equation (12) offers M additional constraints and the solutions of $(\phi_1, \phi_2, \dots, \phi_S)$ form a manifold M_ϕ with dimension $D_2 = D_1 - M = M - (P+1)N_\omega \geq 0$. This analysis gives a lower limit of pulse segments, thus we must have

$$S = 2M \geq 2(P+1)N_\omega. \quad (13)$$

Equation (11) can be directly solved by the Gaussian elimination or any other methods and the basis of W can be written down explicitly

$$\rho^{(d)} = \begin{pmatrix} \rho_X^{(d)} \\ \rho_Y^{(d)} \end{pmatrix}, \quad \rho_X^{(d)} = \begin{pmatrix} \epsilon_{X,1}^{(d)} \\ \epsilon_{X,2}^{(d)} \\ \vdots \\ \epsilon_{X,M}^{(d)} \end{pmatrix}, \quad \rho_Y^{(d)} = \begin{pmatrix} \epsilon_{Y,1}^{(d)} \\ \epsilon_{Y,2}^{(d)} \\ \vdots \\ \epsilon_{Y,M}^{(d)} \end{pmatrix}, \quad (14)$$

where $1 \leq d \leq D_1$. An arbitrary vector in W can be written as

$$\rho = \sum_{d=1}^{D_1} a^{(d)} \rho^{(d)} = \Lambda \mathbf{a}, \quad (15)$$

where $\Lambda = (\rho^{(1)}, \rho^{(1)}, \dots, \rho^{(D_1)})$ is of dimension $2M \times D_1$. The constraints in Eq. (12) then lead to quadratic equations

of $a^{(d)}$:

$$\left(\sum_{d=1}^{D_1} \epsilon_{X,m}^{(d)} a^{(d)} \right)^2 + \left(\sum_{d=1}^{D_1} \epsilon_{Y,m}^{(d)} a^{(d)} \right)^2 - 1 = 0, \quad 1 \leq m \leq M. \quad (16)$$

The Newton method can be applied to efficiently find the solution of Eq. (16) and our goal is to calculate the set of coefficients $\mathbf{a} = (a^{(1)}, a^{(2)}, \dots, a^{(D_1)})^T$. However, the dimension of the Jacobi matrix \mathbf{J} is $M \times D_1$ ($M < D_1$ in our calculations) rather than being a square matrix in the original Newton method. Some trickery is needed to overcome the inconsistency. We can still solve the linear equations related to the Jacobi matrix in each iteration and D_2 linearly independent vectors in W are added to the particular solution. The amplitudes of the added vectors are randomly chosen in a range which is comparable with the particular solution. The randomness introduced here avoids falling into some unfavorable directions. Another consequence is that different results are obtained when we repeatedly carry out the algorithm. Actually, sometimes the iteration cannot converge in a given number of times and we need to restart the algorithm until a solution \mathbf{a} is searched.

C. Power optimization

In the last subsection, we found a way to obtain the laser phases ϕ_s for a fixed Rabi frequency. On this basis, we are also concerned about optimizing the Rabi frequency Ω , which is related to the laser power. Therefore, our next step is to optimize Ω for a searched \mathbf{a} .

Based on Eq. (4), Θ can be expressed in the matrix form as

$$\Theta = \Omega^2 \Phi^T \mathbf{D} \Phi, \quad (17)$$

where \mathbf{D} is a $2M \times 2M$ real symmetric matrix which is independent of Ω and whose elements can be found in Appendix B. Since we obtained the null space W from which \mathbf{a} is constructed, we can thus project \mathbf{D} to W with the transformation matrix Λ , i.e.,

$$\mathbf{D}' = \Lambda^T \mathbf{D} \Lambda, \quad (18)$$

then Eq. (17) becomes

$$\Theta = \Omega^2 \mathbf{a}^T \mathbf{D}' \mathbf{a}. \quad (19)$$

Clearly, we can now use Eq. (19) to calculate Ω for the MS gate, which aims at $|\Theta| = \pi/4$.

Using the above formulation, we can try to find a better solution with a lower power. For this, we have to change \mathbf{a} , while it is difficult to keep Eq. (16) always satisfied. An applicable approach is to search on the tangent space $T_p M_\phi$ of the D_2 -dimension manifold M_ϕ , in which we converted the coordinates $(\phi_1, \phi_2, \dots, \phi_s)$ into \mathbf{a} . Actually, $T_p M_\phi$ is the null space of \mathbf{J} and the orthonormal basis can form a $D_1 \times D_2$ transformation matrix $\tilde{\Lambda}$. The vector in $T_p M_\phi$ can be expressed as

$$\mathbf{a}' = \tilde{\Lambda} \tilde{\mathbf{a}} + \mathbf{a}, \quad (20)$$

where \mathbf{a}' is a D_1 -dimension vector and $\tilde{\mathbf{a}}$ is a small step from \mathbf{a} with the dimension of D_2 . Actually, Eq. (19) inspires us to

calculate

$$\begin{aligned} \theta &\equiv \mathbf{a}'^T \mathbf{D}' \mathbf{a}' \\ &= (\tilde{\Lambda} \tilde{\mathbf{a}} + \mathbf{a})^T \mathbf{D}' (\tilde{\Lambda} \tilde{\mathbf{a}} + \mathbf{a}), \end{aligned} \quad (21)$$

and we want to search a larger θ . The gradient of θ in $T_p M_\phi$ is evaluated to be

$$\nabla_{\tilde{\mathbf{a}}} \theta = 2 \tilde{\Lambda} \mathbf{D}' \mathbf{a}, \quad (22)$$

and we can thus search with a small step in the gradient direction, after which \mathbf{a}' will deviate from M_ϕ a little bit. Now, we can use the above-mentioned Newton method to pull \mathbf{a}' back to M_ϕ .

We can repeat the above process until a convergent θ is searched and thus the power optimal solution \mathbf{a} is found.

III. RESULTS AND DISCUSSIONS

In this section, we will present our main results. Taking a chain of ions as an example, we will first demonstrate the performance of our numerical schemes for a two-qubit phase-modulated MS gate. Then, we will investigate the robustness of the gate. Finally, we will discuss the connectivity and the scalability of our method. Without any specific declaration, the solutions are all power-optimized hereafter.

A. Two-qubit gates

First, we apply our method to a two-qubit gate in a chain of 20 ions. As shown in Fig. 1(a), we assume the MS gate entangles the seventh and the ninth ion (counted from the left) in a chain of 20 $^{171}\text{Yb}^+$ ions along the z axis. First of all, we need to choose the value of D_2 , i.e., the dimension of M_ϕ , which also represents the redundant freedom of the pulse. Actually, a small number of D_2 can significantly simplify the pulse when compared with the conventional optimization method where the redundancy is usually about 50% [21]. Therefore, in our calculations, we take $D_2 = 4$ for a good convergence.

To evaluate the infidelity of the gate given by Eq. (6), an approximation of \bar{n}_k is necessary. In the current experiments, it is not difficult to cool the motional modes to $\bar{n}_k < 0.5$ [32,33] and thus we conservatively assume $\bar{n}_k = 0.5$ in our calculations.

Under the above conditions, laser beams with wavelength $\lambda = 355$ nm are used to manipulate internal states of ions which are encoded in two hyperfine sublevels [2,14]. In our example, the symmetric trap is adopted and the center-of-mass trapping frequencies are taken to be $(\omega_x, \omega_z) = (1.5, 0.1) \times 2\pi$ MHz. The detuning is chosen as $\mu = 2\pi \times 1.305$ MHz, which allows Ω to take a low value, as will be shown below. We consider a phase-modulated pulse with duration $\tau = 300$ μs with the number of pulse segments $S = 88$. In addition, the order of robustness P is taken to be 1.

The phase sequence of the power-optimized solution is shown in Fig. 1(b), from which we can see that the sequence automatically has quite good continuity rather than randomly disperses in $[-\pi, \pi)$. In Fig. 1(c), the iteration of the laser power optimization shows the expected decrease of the Rabi frequency Ω of the pulse.

In Fig. 1(d), we compare the infidelity with and without the power optimization as a function of the drift δ of the

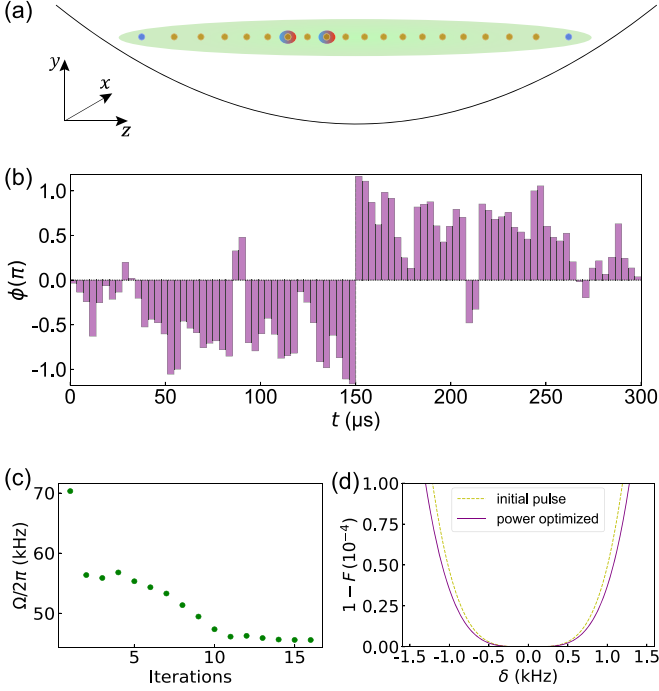


FIG. 1. A phase-modulated MS gate in a chain of 20 ions. (a) Illustration for the trap and laser beams, where the seventh and the ninth ion are entangled (counted from the left). (b) The optimized phase sequence for $\tau = 300 \mu\text{s}$ with $S = 88$. (c) Convergence of the Rabi frequency during the power optimization. Ω falls from $2\pi \times 70 \text{ kHz}$ to $2\pi \times 46 \text{ kHz}$ in 16 iterations. (d) Infidelity as a function of the drift δ of the motional-mode frequency ω_k with and without the power optimization.

motional-mode frequency ω_k . According to Eqs. (3) and (6), we have $1 - F \propto \Omega^2$ and thus we can conclude that the power optimization can increase the robustness of the gate, though the small gain of the robustness is a spin-off of the power optimization. As can be seen from Figs. 1(c) and 1(d), the required Ω is as low as $2\pi \times 46 \text{ kHz}$ and the permitted drift δ of the motional-mode frequency is as large as 1.3 kHz to guarantee $1 - F \leq \epsilon = 10^{-4}$.

B. Optimization and robustness

In the example shown in the previous subsection, the laser detuning μ was carefully selected to be $\mu = 2\pi \times 1.305 \text{ MHz}$, which allows a low Rabi frequency. To see this, in Fig. 2, we show the variation of the Rabi frequency by scanning every μ which satisfies Eq. (8) in a range whose width is twice of the radial frequency. Obviously, Ω acquires a desirable value which is lower than $2\pi \times 50 \text{ kHz}$ when μ is near $2\pi \times 1.3 \text{ MHz}$. In general, our numerical results indicate that the detuning of the best Ω usually appears in the range of the radial frequencies under different parameters.

As for the gate time τ , there are also several points for consideration. Shorter pulses are certainly desirable, but there is a limitation which is decided by the radial frequencies. Specifically, ω_k restricts the rotation of $\alpha_k^j(t)$ in the complex plane, which is also referred to as the phase trajectory. For the cases considered here, the shortest pulse we can achieve

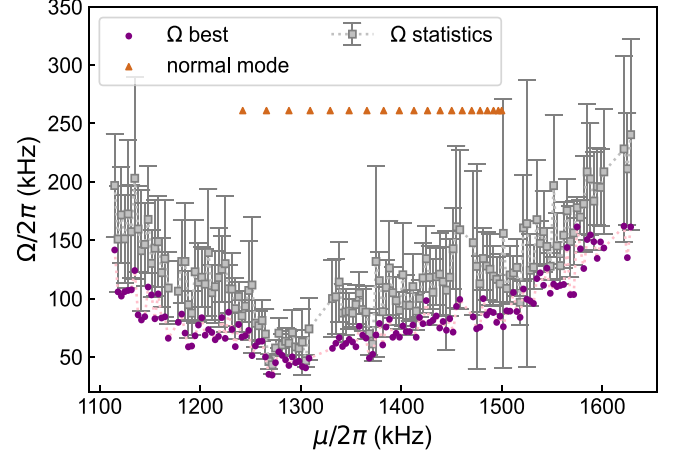


FIG. 2. Rabi frequencies of the pulse sequences calculated at different μ . The calculation is repeated ten times for each μ and the purple dots represent the best Ω for each μ . The gray squares and the error bars are the mean values and the standard deviations of Ω from ten solutions for each μ . The 20 radial frequencies are represented by the orange triangles, scattered in the range of $[1.24, 1.5] \times 2\pi \text{ MHz}$.

is $\tau_{\min} = 196 \mu\text{s}$, as indicated in Fig. 3. Furthermore, we can trade some time for a lower Ω . As can be seen from Fig. 3, Ω quickly decreases with the increase of τ before $\tau_0 = 300 \mu\text{s}$. However, the downtrend of Ω slows down after τ_0 , which is the reason why we chose $\tau = \tau_0$ for the results presented in Fig. 1.

It will be instructive to see the success chance of finding an optimal Rabi frequency for a given pulse duration τ , which is also shown in Fig. 3. Here we define the success rate as the ratio of the number of searched solutions and the total starts of the algorithm. As can be seen, our algorithm ensures a continuous growth of the success rate when $\tau \in [\tau_{\min}, \tau_0]$. Although the fast growth terminates when $\tau > \tau_0$, the algorithm

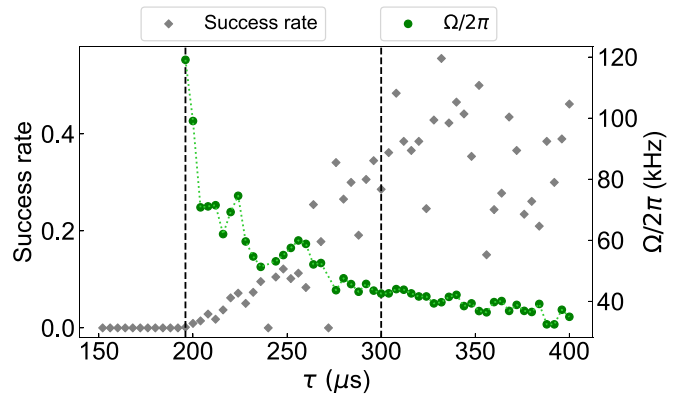


FIG. 3. Success rate of the algorithm and Rabi frequencies for different gate time τ . The calculation is repeated for ten times with each τ , and each time one permits a maximum number of 50 for the restarts before a success. Gray diamonds are the success rate and green dots show the best Rabi frequencies of the obtained solutions for each τ . Two vertical dashed lines, respectively, represent the shortest gate time $\tau_{\min} = 196 \mu\text{s}$ in our calculations and the suitable gate time $\tau_0 = 300 \mu\text{s}$.

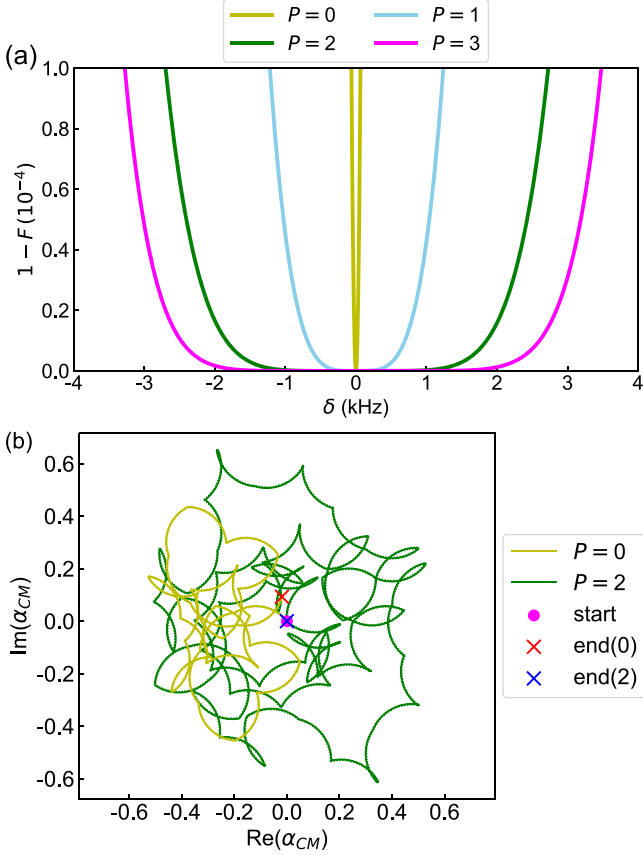


FIG. 4. Robustness of the gates for $N = 10$. (a) Infidelity against the frequency drift for $P = 0, 1, 2, 3$. (b) Phase trajectories of COM for $P = 0, 2$. The purple dot represents the common start, e.g., $\alpha_{COM}(0) = 0$. The red cross and the blue cross are the ends of the trajectories for $P = 0, 2$, respectively. We suppose that the internal states of the two qubits j_1, j_2 are both $|+\rangle$ and the excitation of COM is $\alpha_{COM} = \alpha_{COM}^{j_1} + \alpha_{COM}^{j_2}$ where $j_1 = 2$ and $j_2 = 4$. The detuning is changed to $\mu = 2\pi \times 1.468$ MHz due to the change of the ion number.

maintains a high success rate and thus the required computing resource is not demanding.

Having discussed the optimal parameters μ and τ for the experimental feasibility, we now turn to the robustness of the phase-modulated MS gates. According to Eqs. (7), (9), and (11), we can readily increase the robustness of the gate by using a larger P in our algorithm.

For this purpose, we investigate the infidelity as a function of δ with $P = (0, 1, 2, 3)$ for the gate which entangles the second and the fourth ion in a chain of $N = 10$ in a symmetric trap. It should be mentioned that we reduced N to show the phase trajectories clearly. The resultant robustness against the frequency drift is visualized in Fig. 4(a). Obviously, the corresponding width of δ for the infidelity smaller than $\epsilon = 10^{-4}$ increases from 0.1 kHz to more than 3 kHz when P changes from 0 to 3.

Of course, we should note that τ has to be longer for a larger P because a too-short pulse cannot support the phase trajectory to be complicated enough to satisfy the high robustness constraints. Meanwhile, Eq. (13) tells us that the segments of the pulse will also increase with P .

In our calculations shown in Fig. 4(a), τ is taken to be (200, 300, 450, 800) μs for $P = (0, 1, 2, 3)$, respectively, and the corresponding Ω is (49, 44, 52, 22) $\times 2\pi$ kHz for each case. Note that the enhancement of the robustness does not necessarily increase Ω and sometimes Ω even declines due to a longer τ . In addition, τ is chosen as the minimal multiple of 50 μs where the successful rate is obviously larger than 0 for each P .

To intuitively show the evidence of the effectiveness of the robust scheme, in Fig. 4(b), we plot the phase trajectories of the center-of-mass mode (COM) for $P = 0, 2$ with $\delta = 2$ kHz. We can notice that the trajectory for $P = 0$ deviates from the start after the gate operation, while the one for $P = 2$ returns to the start without visible difference, which demonstrates the robustness of the gate.

C. Connectivity and scalability

Connectivity is an important issue in a quantum gate. To explore the connectivity of our scheme, we search the solutions for every pair of ions (j_1, j_2) in a chain of 20 ions. In Figs. 5(a) and 5(b), we show the infidelity and the Rabi frequency, respectively. Obviously, the outermost squares are brighter, which means that the gates related to the first or the 20th ion have the worse robustness and also need a higher laser power. This is why the ions in the edge of the ion chain are usually regarded as buffer ions, which do not participate in the computing [2]. In the middle of Figs. 5(a) and 5(b), the color is relatively even, indicating the convenience to operate any pair in the middle of the chain.

As mentioned previously, the major advantage of our numerical method is the scalability for a long chain. We explored the scalability for both the symmetric and the asymmetric traps, while the latter are more time consuming for a same N due to more modes to be disentangled. The solutions for the gates up to $N = 20$ were obtained in previous studies for the asymmetric trap [21,26], while it is increased to 35 with our method. For the symmetric trap, N can be further improved to 60 in this work. In Fig. 6(a), we present the averaged time consumption for the initial solution t_1 and for the power optimization t_2 with different N . The center-of-mass trapping frequencies are still chosen as $(\omega_x, \omega_z) = (1.5, 0.1) \times 2\pi$ MHz for $N \leq 26$ in the symmetric trap, but ω_x is adjusted to set the highest radial mode equal to the highest axial mode for $N > 26$ to avoid the transition from a chain to a zigzag configuration [34], which keeps the lowest radial mode away from 0. For the asymmetric trap, we can safely choose $\omega_y = 1.1\omega_x$. For both cases, the gate time τ is chosen as 400 μs and the detuning μ is selected according to the optimal proportion in the radial frequencies in Fig. 2. We also choose the ion with number j_1 near the middle one (or two) in the chain and $j_2 = j_1 - 2$ to be entangled just as the cases shown in Figs. 1 and 4.

As can be seen, for a large-enough N the time consumption t_1 will dominate over t_2 for both the symmetric and asymmetric trap. It is worth pointing out that our algorithm can obtain the laser-optimized solution within 1 hour for $N < 43$ (28) for the symmetric (asymmetric) case, in which the calculations are carried out on one core of a server with 2.10-GHz Intel Xeon Silver 4110 CPUs.

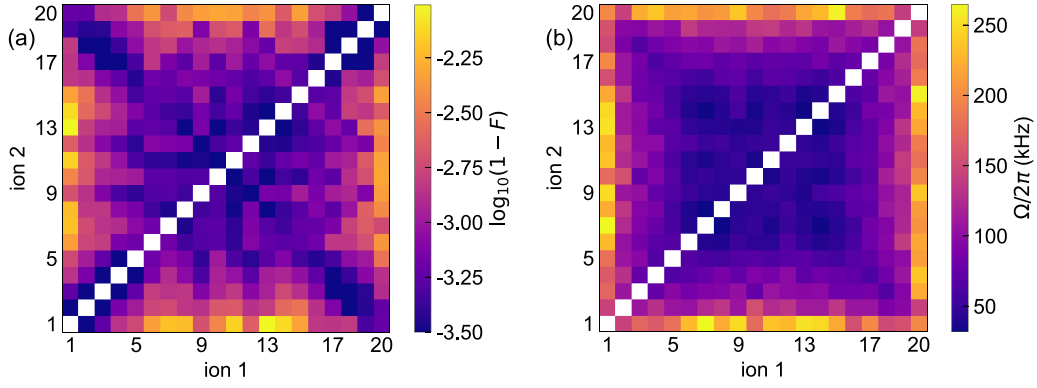


FIG. 5. Connectivity of the gates. (a) Infidelity when $\delta = 2$ kHz and (b) Rabi frequency for each pair of ions (j_1, j_2) in a chain of 20 ions. The pairs which contain the edge ions, e.g., numbered as 1 and 20, have a poor performance of either the robustness or the Rabi frequency, so they are usually not used in experiments. Other parameters, including $\mu, \tau, \omega_{x,z}$, are identical to those of the calculations in Fig. 1.

It is important to see how the infidelity and the Rabi frequency change against the increase of N . In Figs. 6(b) and 6(c), we, respectively, present the infidelity with the motional-mode frequency drift $\delta = 2$ kHz and the Rabi frequency for N ranging from 8 to 60 (35) in the symmetric (asymmetric) trap. In practice, we repeated our calculations for ten times (not each one is successful especially for large N) and then we choose the minima to be shown. It is inspiring to see that the infidelity does not increase with N and disperses in the range of 10^{-2} – 10^{-3} . Although the Rabi frequency Ω slightly increases with N and it keeps less than $2\pi \times 200$ kHz in the chosen range of N , which is realizable in current experiments.

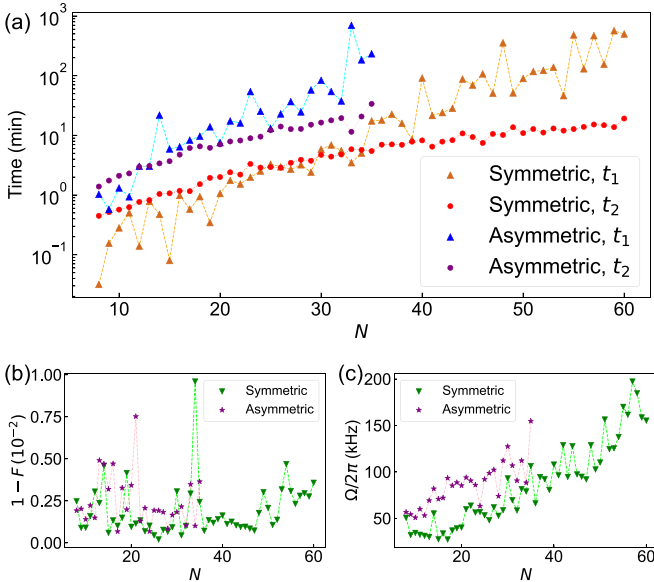


FIG. 6. Scalability of the current numerical method. (a) Scaling of the computation time for a single solution of both the symmetric and the asymmetric trap. The algorithm has a good convergence up to $N = 60$ (35) for the symmetric (the asymmetric) trap. (b) Infidelity of the gates when motional-mode frequencies have a uniform drift $\delta = 2$ kHz. (c) Rabi frequency for different N . Each calculation is performed on one core of a server with 2.10-GHz Intel Xeon Silver 4110 CPUs.

IV. CONCLUSION

We demonstrated a scalable numerical framework for the phase-modulated MS gates. We showed that the reduction to linear algebra and the root finding of quadratic equations largely improves both the convergence of the algorithm and the performance of the gates. By using the present scheme, we successfully searched the solutions with the fidelity equal to 1 very efficiently for up to 60 ions, while the robustness against the motional-mode frequency drift and the laser power can be maintained in desirable conditions for experiments. We explored the most appropriate parameters for experiments, such as the gate time and the Rabi frequency.

The current algorithm can be potentially extended to the motional heating, which is a critical error source [35]. Other experimental errors, such as laser fluctuations and high-order effects of Lamb-Dicke parameters [31], can also be included. With the increasing number of ions which can be coherently operated for the quantum computing in future experiments, we believe that our framework can be applied to find optimal schemes available for the phase-modulated MS gates.

ACKNOWLEDGMENT

This work is supported by National Natural Science Foundation of China under Grants No. 12234002 and No. 92250303.

APPENDIX A: PULSE SYMMETRY

With the odd parity of $\phi(t)$ and the constraint of μ in Eq. (8), the number of real constraints in Eq. (7) can be reduced by half. We recover the integration from 0 to τ of Eq. (7) for clarity and reformulate the expression

$$\begin{aligned}
 0 &= \int_0^\tau t^p \sin[\mu t + \phi(t)] e^{i\omega_k t} dt \\
 &= e^{i\omega_k \frac{\tau}{2}} \sum_{p'=0}^p C_{p'}^p (-1)^{p'} \left(\frac{\tau}{2}\right)^{p-p'} \\
 &\quad \times \int_0^\tau \left(\frac{\tau}{2} - t\right)^{p'} \sin[\mu t + \phi(t)] e^{i\omega_k(t-\frac{\tau}{2})} dt. \quad (\text{A1})
 \end{aligned}$$

Here we can use the idea of mathematical induction. If the robustness conditions of less than the p th order are satisfied, the p th order will only add the following new equations:

$$\int_0^\tau \left(\frac{\tau}{2} - t\right)^p \sin[\mu t + \phi(t)] e^{i\omega_k(t - \frac{\tau}{2})} dt = 0. \quad (\text{A2})$$

The above-mentioned symmetric constraints of the pulse leads to the parity of the integrand in Eq. (A2): if p is even, the real part of the integrand is even about the midpoint $\frac{\tau}{2}$, while the imaginary part is odd, and vice versa if p is odd. The result of the integral is always 0 for the odd integrands, so we need only the other half of the equations for any p :

$$\begin{aligned} \int_0^{\frac{\tau}{2}} t^p \cos\left[\mu t - \phi\left(\frac{\tau}{2} - t\right)\right] \cos(\omega_k t) dt &= 0, \\ p = 2N_p \leq P, \quad k = 1, 2, \dots, N_\omega; \\ \int_0^{\frac{\tau}{2}} t^p \cos\left[\mu t - \phi\left(\frac{\tau}{2} - t\right)\right] \sin(\omega_k t) dt &= 0, \\ p = 2N_p + 1 \leq P, \quad k = 1, 2, \dots, N_\omega, \end{aligned} \quad (\text{A3})$$

which can be rewritten as Eq. (9) if the phase is segmented. The default condition $N_p \in \mathbb{N}$ is omitted here and below.

APPENDIX B: MATRIX OF CONSTRAINTS

Based on Eq. (9), we can easily write down the matrix elements for the coefficient matrix \mathbf{M} :

$$\begin{aligned} (\mathbf{M}_X^p)_{k,M-s} &= \begin{cases} \int_{t_s}^{t_{s+1}} t^p \cos(\mu t) \cos(\omega_k t) dt, & p = 2N_p, \\ \int_{t_s}^{t_{s+1}} t^p \cos(\mu t) \sin(\omega_k t) dt, & p = 2N_p + 1; \end{cases} \\ (\mathbf{M}_Y^p)_{k,M-s} &= \begin{cases} \int_{t_s}^{t_{s+1}} t^p \sin(\mu t) \cos(\omega_k t) dt, & p = 2N_p, \\ \int_{t_s}^{t_{s+1}} t^p \sin(\mu t) \sin(\omega_k t) dt, & p = 2N_p + 1, \end{cases} \end{aligned} \quad (\text{B1})$$

where $0 \leq s \leq M - 1$.

Similarly, from Eqs. (4) and (19), we can obtain the elements for \mathbf{D} . It is convenient to decompose \mathbf{D} to $(\mathbf{D}_0 + \mathbf{D}_0^T)/2$, where \mathbf{D}_0 is concatenated with four $M \times M$ lower triangular matrices

$$\mathbf{D}_0 = \begin{pmatrix} \mathbf{D}_{XX} & \mathbf{D}_{XY} \\ \mathbf{D}_{YX} & \mathbf{D}_{YY} \end{pmatrix}. \quad (\text{B2})$$

The explicit expressions of these matrices are

$$\begin{aligned} (\mathbf{D}_{XX})_{ss} &= \left(2 \int_{t_{s-1}}^{t_s} \int_{t_{s-1}}^{t_\alpha} + 1 \int_{t_{S-s}}^{t_{S-s+1}} \int_{t_{s-1}}^{t_s}\right) dt_\alpha dt_\beta \sum_k \xi_k \sin[\omega_k(t_\alpha - t_\beta)] \sin(\mu t_\alpha) \sin(\mu t_\beta), \\ (\mathbf{D}_{XX})_{ss'} &= \left(\int_{t_{s-1}}^{t_s} \int_{t_{s'-1}}^{t_{s'}} + \int_{t_{S-s}}^{t_{S-s+1}} \int_{t_{s'-1}}^{t_{s'}}\right) dt_\alpha dt_\beta \sum_k 2\xi_k \sin[\omega_k(t_\alpha - t_\beta)] \sin(\mu t_\alpha) \sin(\mu t_\beta), \\ (\mathbf{D}_{XY})_{ss} &= \left(2 \int_{t_{s-1}}^{t_s} \int_{t_{s-1}}^{t_\alpha} + 1 \int_{t_{S-s}}^{t_{S-s+1}} \int_{t_{s-1}}^{t_s}\right) dt_\alpha dt_\beta \sum_k \xi_k \sin[\omega_k(t_\alpha - t_\beta)] \sin(\mu t_\alpha) \cos(\mu t_\beta), \\ (\mathbf{D}_{XY})_{ss'} &= \left(\int_{t_{s-1}}^{t_s} \int_{t_{s'-1}}^{t_{s'}} + \int_{t_{S-s}}^{t_{S-s+1}} \int_{t_{s'-1}}^{t_{s'}}\right) dt_\alpha dt_\beta \sum_k 2\xi_k \sin[\omega_k(t_\alpha - t_\beta)] \sin(\mu t_\alpha) \cos(\mu t_\beta), \\ (\mathbf{D}_{YX})_{ss} &= \left(2 \int_{t_{s-1}}^{t_s} \int_{t_{s-1}}^{t_\alpha} - 1 \int_{t_{S-s}}^{t_{S-s+1}} \int_{t_{s-1}}^{t_s}\right) dt_\alpha dt_\beta \sum_k \xi_k \sin[\omega_k(t_\alpha - t_\beta)] \cos(\mu t_\alpha) \sin(\mu t_\beta), \\ (\mathbf{D}_{YX})_{ss'} &= \left(\int_{t_{s-1}}^{t_s} \int_{t_{s'-1}}^{t_{s'}} - \int_{t_{S-s}}^{t_{S-s+1}} \int_{t_{s'-1}}^{t_{s'}}\right) dt_\alpha dt_\beta \sum_k 2\xi_k \sin[\omega_k(t_\alpha - t_\beta)] \cos(\mu t_\alpha) \sin(\mu t_\beta), \\ (\mathbf{D}_{YY})_{ss} &= \left(2 \int_{t_{s-1}}^{t_s} \int_{t_{s-1}}^{t_\alpha} - 1 \int_{t_{S-s}}^{t_{S-s+1}} \int_{t_{s-1}}^{t_s}\right) dt_\alpha dt_\beta \sum_k \xi_k \sin[\omega_k(t_\alpha - t_\beta)] \cos(\mu t_\alpha) \cos(\mu t_\beta), \\ (\mathbf{D}_{YY})_{ss'} &= \left(\int_{t_{s-1}}^{t_s} \int_{t_{s'-1}}^{t_{s'}} - \int_{t_{S-s}}^{t_{S-s+1}} \int_{t_{s'-1}}^{t_{s'}}\right) dt_\alpha dt_\beta \sum_k 2\xi_k \sin[\omega_k(t_\alpha - t_\beta)] \cos(\mu t_\alpha) \cos(\mu t_\beta), \end{aligned} \quad (\text{B3})$$

where $s' < s$ and $\xi_k = 2\eta_k^2 b_k^i b_k^j$. The integrals in Eqs. (B1) and (B3) can be analytically calculated, so this step is not time consuming.

[1] P. Wang, C.-Y. Luan, M. Qiao, M. Um, J. Zhang, Y. Wang, X. Yuan, M. Gu, J. Zhang, and K. Kim, *Nat. Commun.* **12**, 233 (2021).
 [2] K. Wright, K. M. Beck, S. Debnath, J. M. Amini, Y. Nam, N. Grzesiak, J.-S. Chen, N. C. Pisenti, M. Chmielewski, C. Collins,

K. M. Hudek, J. Mizrahi, J. D. Wong-Campos, S. Allen, J. Apisdorf, P. Solomon, M. Williams, A. M. Ducore, A. Blinov, S. M. Kreikemeier *et al.*, *Nat. Commun.* **10**, 5464 (2019).
 [3] S. Debnath, N. M. Linke, C. Figgatt, K. A. Landsman, K. Wright, and C. Monroe, *Nature (London)* **536**, 63 (2016).

- [4] C. J. Ballance, T. P. Harty, N. M. Linke, M. A. Sepiol, and D. M. Lucas, *Phys. Rev. Lett.* **117**, 060504 (2016).
- [5] J. P. Gaebler, T. R. Tan, Y. Lin, Y. Wan, R. Bowler, A. C. Keith, S. Glancy, K. Coakley, E. Knill, D. Leibfried, and D. J. Wineland, *Phys. Rev. Lett.* **117**, 060505 (2016).
- [6] I. Pogorelov, T. Feldker, C. D. Marciniak, L. Postler, G. Jacob, O. Kriegelsteiner, V. Podlesnic, M. Meth, V. Negnevitsky, M. Stadler, B. Höfer, C. Wächter, K. Lakhmanskii, R. Blatt, P. Schindler, and T. Monz, *PRX Quantum* **2**, 020343 (2021).
- [7] T. Choi, S. Debnath, T. A. Manning, C. Figgatt, Z.-X. Gong, L.-M. Duan, and C. Monroe, *Phys. Rev. Lett.* **112**, 190502 (2014).
- [8] K. A. Landsman, Y. Wu, P. H. Leung, D. Zhu, N. M. Linke, K. R. Brown, L. Duan, and C. Monroe, *Phys. Rev. A* **100**, 022332 (2019).
- [9] C. D. Bruzewicz, R. McConnell, J. Chiaverini, and J. M. Sage, *Nat. Commun.* **7**, 13005 (2016).
- [10] S. T. Wang, C. Shen, and L. M. Duan, *Sci. Rep.* **5**, 8555 (2015).
- [11] Y.-K. Wu, Z.-D. Liu, W.-D. Zhao, and L.-M. Duan, *Phys. Rev. A* **103**, 022419 (2021).
- [12] H. Kaufmann, T. Ruster, C. T. Schmiegelow, M. A. Luda, V. Kaushal, J. Schulz, D. von Lindenfels, F. Schmidt-Kaler, and U. G. Poschinger, *Phys. Rev. Lett.* **119**, 150503 (2017).
- [13] H. N. Tinkey, C. R. Clark, B. C. Sawyer, and K. R. Brown, *Phys. Rev. Lett.* **128**, 050502 (2022).
- [14] Y. Lu, S. N. Zhang, K. Zhang, W. T. Chen, Y. C. Shen, J. L. Zhang, J. N. Zhang, and K. Kim, *Nature (London)* **572**, 363 (2019).
- [15] G. Pagano, P. W. Hess, H. B. Kaplan, W. L. Tan, P. Richerme, P. Becker, A. Kyprianidis, J. Zhang, E. Birkelbaw, M. R. Hernandez, Y. Wu, and C. Monroe, *Quantum Sci. Technol.* **4**, 014004 (2018).
- [16] A. Sørensen and K. Mølmer, *Phys. Rev. Lett.* **82**, 1971 (1999).
- [17] A. Sørensen and K. Mølmer, *Phys. Rev. A* **62**, 022311 (2000).
- [18] S.-L. Zhu, C. Monroe, and L.-M. Duan, *Europhys. Lett.* **73**, 485 (2006).
- [19] Y. Wu, S.-T. Wang, and L.-M. Duan, *Phys. Rev. A* **97**, 062325 (2018).
- [20] T. J. Green and M. J. Biercuk, *Phys. Rev. Lett.* **114**, 120502 (2015).
- [21] A. R. Milne, C. L. Edmunds, C. Hempel, F. Roy, S. Mavadia, and M. J. Biercuk, *Phys. Rev. Appl.* **13**, 024022 (2020).
- [22] P. H. Leung, K. A. Landsman, C. Figgatt, N. M. Linke, C. Monroe, and K. R. Brown, *Phys. Rev. Lett.* **120**, 020501 (2018).
- [23] M. Kang, Q. Liang, B. Zhang, S. Huang, Y. Wang, C. Fang, J. Kim, and K. R. Brown, *Phys. Rev. Appl.* **16**, 024039 (2021).
- [24] P. H. Leung and K. R. Brown, *Phys. Rev. A* **98**, 032318 (2018).
- [25] R. Blümel, N. Grzesiak, N. Pisenti, K. Wright, and Y. Nam, *npj Quantum Inf.* **7**, 147 (2021).
- [26] C. D. B. Bentley, H. Ball, M. J. Biercuk, A. R. R. Carvalho, M. R. Hush, and H. J. Slatyer, *Adv. Quantum Technol.* **3**, 2000044 (2020).
- [27] P. J. Lee, K.-A. Brickman, L. Deslauriers, P. C. Haljan, L.-M. Duan, and C. Monroe, *J. Opt. B: Quantum Semiclassical Opt.* **7**, S371 (2005).
- [28] S.-L. Zhu, C. Monroe, and L.-M. Duan, *Phys. Rev. Lett.* **97**, 050505 (2006).
- [29] D. F. V. James, *Appl. Phys. B: Lasers Opt.* **66**, 181 (1998).
- [30] S. C. Doret, J. M. Amini, K. Wright, C. Volin, T. Killian, A. Ozakin, D. Denison, H. Hayden, C.-S. Pai, R. E. Slusher, and A. W. Harter, *New J. Phys.* **14**, 073012 (2012).
- [31] K. Wang, J.-F. Yu, P. Wang, C. Luan, J.-N. Zhang, and K. Kim, *Quantum Sci. Technol.* **7**, 044005 (2022).
- [32] B. P. Ruzic, T. A. Barrick, J. D. Hunker, R. J. Law, B. K. McFarland, H. J. McGuinness, L. P. Parazzoli, J. D. Sterk, J. W. Van Der Wall, and D. Stick, *Phys. Rev. A* **105**, 052409 (2022).
- [33] A. E. Webb, S. C. Webster, S. Collingbourne, D. Bretaudo, A. M. Lawrence, S. Weidt, F. Mintert, and W. K. Hensinger, *Phys. Rev. Lett.* **121**, 180501 (2018).
- [34] S. Fishman, G. De Chiara, T. Calarco, and G. Morigi, *Phys. Rev. B* **77**, 064111 (2008).
- [35] F. Haddadfarshi and F. Mintert, *New J. Phys.* **18**, 123007 (2016).